We are IntechOpen,
the world's leading publisher of
Open Access books
Built by scientists, for scientists

4,800
Open access books available

122,000
International authors and editors

135M
Downloads

Our authors are among the

154
Countries delivered to

TOP 1%
most cited scientists

12.2%
Contributors from top 500 universities

BOOK
CITATION
INDEX
CLARIVATE ANALYTICS
INDEXED

WEB OF SCIENCE™

Selection of our books indexed in the Book Citation Index
in Web of Science™ Core Collection (BKCI)

Interested in publishing with us?
Contact book.department@intechopen.com

Numbers displayed above are based on latest data collected.
For more information visit www.intechopen.com

Ion Implantation in Phase Change Ge$_2$Sb$_2$Te$_5$ Thin Films for Non Volatile Memory Applications

Stefania Maria Serena Privitera
Consiglio Nazionale delle Ricerche (CNR)
Istituto di Microelettronica e Microsistemi (IMM)
Catania
Italy

1. Introduction

Phase change materials are characterized by the existence of at least two different phases, between which it is possible to reversibly and repeatedly switch in a very short timescale. Large variation of the electrical and optical properties occurs upon phase change. These unique properties have made phase change materials very attractive for the realization of nonvolatile electronic memories based on the concept of using the reversible amorphous-to-crystalline phase transition as writing and erasing mechanism. The two logic states are the high resistance, low reflectivity amorphous phase and the crystalline, high reflectivity, low resistance phase. The switching can be obtained either by using a laser pulse or an electric pulse.

The technological success of phase change materials was firstly linked to the realization of optical memories, and it was enabled by the discovery of a class of materials, belonging to the pseudobinary line GeTe-Sb$_2$Te$_3$, characterized by large variation of optical contrast by laser pulses. Thanks to the use of such materials, the rewritable optical storage technology has been developed, reaching its third generation of blu-ray disks with 100 Gb capacity. The most common used material for optical disks has composition Ge$_2$Sb$_2$Te$_5$ and it is also characterized by order of magnitude of resistance variation when changing from amorphous to polycrystal, with face centered cubic structure (*fcc*). Following the optical memory concept, the phase change materials have been proposed for the realization of nonvolatile memories based on the phase transitions driven by electric pulses. Phase change memories (PCM) employing Ge$_2$Sb$_2$Te$_5$ as recording media have been successfully manufactured, obtaining large electrical contrast, with orders of magnitude of difference between the resistance in amorphous and crystalline phase (Lai & Lowrey, 2001; Redaelli & Pirovano, 2011).

Many material aspects have to be taken into account for the realization of phase change electrical memories. One limits the application of phase change memories as multi-level memory, and it is the drift effect of the amorphous phase resistance, i.e. a resistance increase occurring even at room temperature. The second major issue is due to the low crystallization temperature of the amorphous phase, which may limit the data retention under operation conditions and therefore the reliability of phase change memories that should be stable in

the amorphous phase for ten years at 80°C for embedded applications and at 150°C for automotive applications.

In this chapter we will show how ion beam can be employed as a useful tool to investigate and modify some physical properties of phase change materials. In particular we will focus on the stability of the amorphous phase, the data retention properties and the crystallization time, that represents the most limiting time constant.

2. Phase change memory

In phase change memories (PCM) the write and erasing mechanisms are based on the reversible amorphous-to-crystal transition, being the two logic states the amorphous and the *fcc* polycrystalline phase. Data reading is performed by measuring the resistance of the Ge-Sb-Te cell, without producing any phase transition.

The crystallization of the amorphous material (SET operation) is obtained through Joule heating by current pulses but it is enabled by a threshold switching mechanism which allows enough current to flow through the material to heat it above crystallization temperature. The threshold switching occurs at a certain threshold field, on the order of 10-100 V/μm (Krebs et al., 2009), depending on the material composition, and it is characterized by a sudden decrease of resistivity, with negative differential resistance, as schematically shown in figure 1. Several models have been suggested to explain this effect, such as thermal runaway caused by Joule heating (Owen et al. 1979) or energy gain of electrons in a high electric field, leading to a voltage-current instability (Ielmini, 2008). However, detailed experimental validations of the proposed models are further required to better understand the physical mechanisms.

It is experimentally observed that the threshold switching is a reversible phenomenon. If a short voltage pulse above the switching threshold is applied and quickly removed, after a short delay time, the memory cell returns to the high resistance value of the amorphous state, without memory switching. If the voltage pulse is long enough to heat the material above the crystallization temperature, the conversion into the crystalline phase occurs, and after pulse the cell has low resistance.
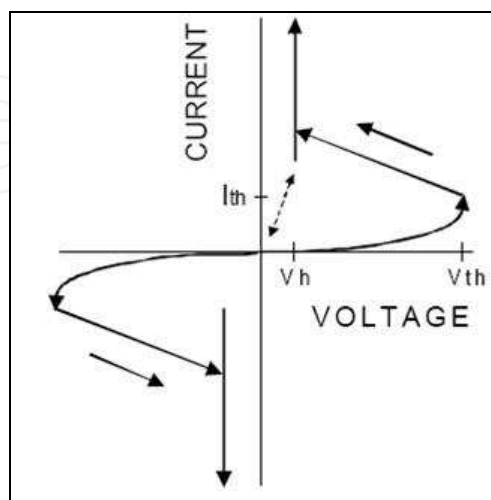

Fig. 1. Current-voltage characteristic of a phase change material, exhibiting electronic threshold switching.

The amorphous-to-crystal transformation is a first order phase transition governed by nucleation and growth and its investigation is crucial for memory applications since the most limiting time constant is the crystallization time and the reliability and retention properties strongly depend on the crystallization kinetics.

To increase the crystallization temperature (~150°C) adversely affecting the retention properties, nitrogen doped Ge$_2$Sb$_2$Te$_5$ (GST) has been proposed for PCM (Horii et al., 2003). In fact, it has been shown that nitrogen doping during deposition (Kojima et al. 1998, Jeong et al. 2000) increases the amorphous stability and reduces the grain size, improving the cell cyclability.

The erasing operation (RESET) is achieved through the crystal-to-amorphous phase transition. Amorphization of crystalline films can be obtained by melting and quenching of the melt fast enough that it solidifies in the amorphous state or by ion implantation at room temperature, producing films of various properties (Mio et al. 2010, Raoux et al. 2010). In nonvolatile electrical memory cells melt quenching is obtained by applying a high and short voltage pulse that melts the material, while in optical memories laser pulses are employed. In PCM devices, after melt quenching, the material usually undergoes structural relaxation leading to a resistance drift to higher values over time. This amorphous instability has not been yet understood and it has been explained by considering stress release (Pirovano et al. 2004, Boniardi et al. 2009), decrease of defect density (Ielmini, 2008), shift of the Fermi level or increase of the band gap (Pirovano et al., 2004). Indeed, it has been shown that amorphous phase change materials can have very different properties depending on the way they are produced (melt quenching, room temperature deposition or ion implantation) and on their thermal history (Lee et al., 2009, De Bastiani et al., 2008).

We will investigate the effect of ion beam on the electrical properties of amorphous Ge$_2$Sb$_2$Te$_5$ thin films by comparing the electrical properties of deposited amorphous materials to melt-quenched films obtained by laser pulses irradiation and to films amorphized by ion implantation.

Ion implantation has been also employed to introduce impurities belonging to different groups (nitrogen, oxygen and fluorine) into amorphous GST films, in order to produce films with different physical properties. The effects of doping on the electrical conduction of amorphous material and on the amorphous -to-crystal transition will be shown.

3. Amorphization by ion beam

In order to study the crystal-to-amorphous transition we have prepared crystalline films, 70 nm thick, by RF sputtering at 250°C from a single target, on a 500nm thick SiO$_2$ film, deposited by chemical vapour deposition on a Si substrate.

The film stoichiometry was measured by electron Auger spectroscopy and energy dispersion X-ray spectrometry (EDXS). X-ray diffraction (XRD) indicated the deposited samples were crystalline.

Amorphization was obtained either by ion implantation or laser melt quenching. For ion implantation, samples were obtained by implanting Ge at 130KeV with a dose of 9e13/cm². This dose corresponds to 0.08 % of Ge in the film, and therefore it is low enough to not alter the film composition but it is effective to amorphize the material. Indeed, after implantation,

the XRD spectrum was typical of an amorphous phase and the electrical resistivity was comparable to that measured in the as deposited amorphous film. The complete amorphization was detected by X-ray diffraction in glancing angle, to enhance the signal from the thin phase change layer. XRD measurements have been carried out using a SIEMENS D5005 diffractometer operating with Cu K_α (λ =0.15406 nm). The X-ray beam was incident at 0.7° on the sample surface and the detector angle was incremented with an angular step of 0.02°. Figure 2 shows in red the XRD spectra of 70 nm thick crystalline films, as deposited at 250°C, with typical rocksalt patterns, and, in blue, the same film after ion implantation of Ge. No XRD peak is visible anymore and the pattern is typical of amorphous materials.
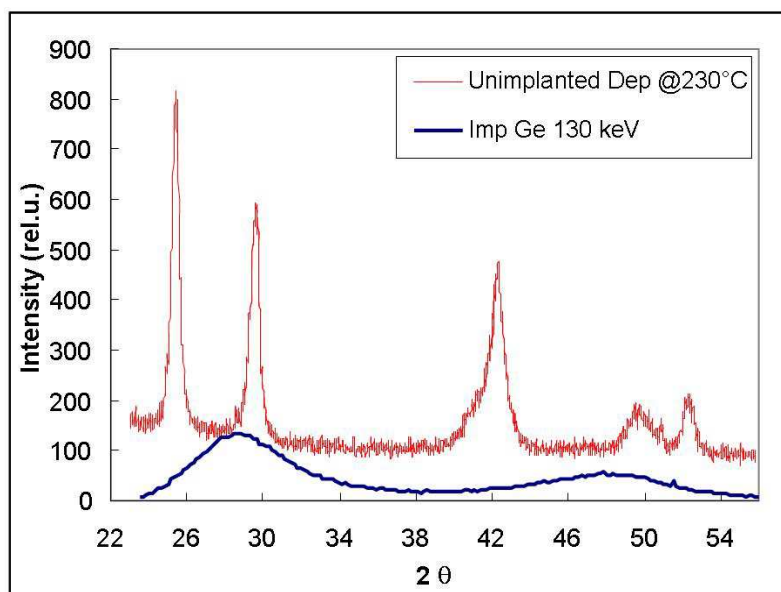

Fig. 2. XRD spectra of $Ge_2Sb_2Te_5$ deposited at 250°C, in the rocksalt structure (red), and after ion implantation with Ge at 130KeV, 9e13/cm² (blue). After implantation the XRD peak is typical of an amorphous material.
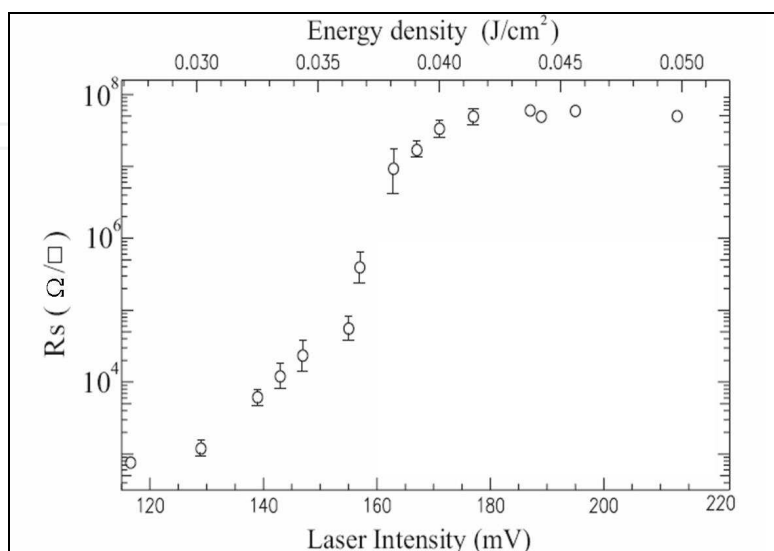

Fig. 3. Sheet resistance of melt quenched crystalline films versus laser intensity. The higher sheet resistance is measured in completely amorphized films.

Melt-quenched films were obtained by using a Ruby laser operating at 695nm. Samples were irradiated with a 30 ns laser pulse, employing a spot diameter of 3.5 mm. The energy density was varied and the effect of film irradiation was monitored by measuring the sheet resistance using a four point probe.

Figure 3 shows the sheet resistance as a function of laser intensity. Below 30 mJ/cm² the measured sheet resistance is around 1000Ohm/square, typical of crystalline GST. This value gradually increases with laser intensity and reaches a saturation value of 5E7 Ohm/square for energy densities above 40mJ/cm².

Data shown in fig. 3 can be explained by considering the depth of melt versus energy density. The heating and melting produced by the laser pulse can be described by considering the heat diffusion equation with the addition of a source term driven by the absorption of laser radiation (Baeri, 1982). If the film is spatially uniform, then away from the edges of the irradiated area any temperature variation will occur only along the axis perpendicular to the sample surface. This simplifies the problem to one dimension and it is described by the equation

$$\frac{\partial T}{\partial t} = \frac{\alpha}{\rho C_p} I(z,t) + \frac{1}{\rho C_p} \frac{\partial}{\partial z}\left(\kappa \frac{\partial T}{\partial z}\right) \tag{1}$$

where T is the temperature at time t and depth z, α is the absorption coefficient of the illuminated material, with specific heat capacity C_p and density ρ, κ is the thermal conductivity and I is the laser power density.

$$I(t,z) = I_0(t)\ (1\text{-}R)\ exp(\text{-}\alpha z) \tag{2}$$

For the same laser pulse duration, the melt region depth can be calculated by dividing the sample into slices of thickness Δz and discretising time into units Δt. The temperature of each slice is then calculated from the energy deposited into the material by absorption of laser light and heat transfer by diffusion. The parameters used for calculations are shown in table 1.

Melting Temperature (K)	891
Thermal Diffusivity (cm²/s)	4.7e-3
Thermal conductivity (W/cm)	0.582e-2
Specific Heat (J/cm³ K)	1.2
Density (g/cm³)	6.2
Latent Heat of fusion (J/cm³)	600

Table 1. Parameters used for numerical calculations of the depth of melting region under irradiation by a 30 ns laser pulse

The results of simulations are shown in figure 4, where the melt depth is plotted as a function of time for different energy densities. According to the measured sheet resistance no melting, which means no amorphization, is expected for energy density below 30mJ/cm². For energy densities above this threshold value, the melting depth increases as the energy density increases.
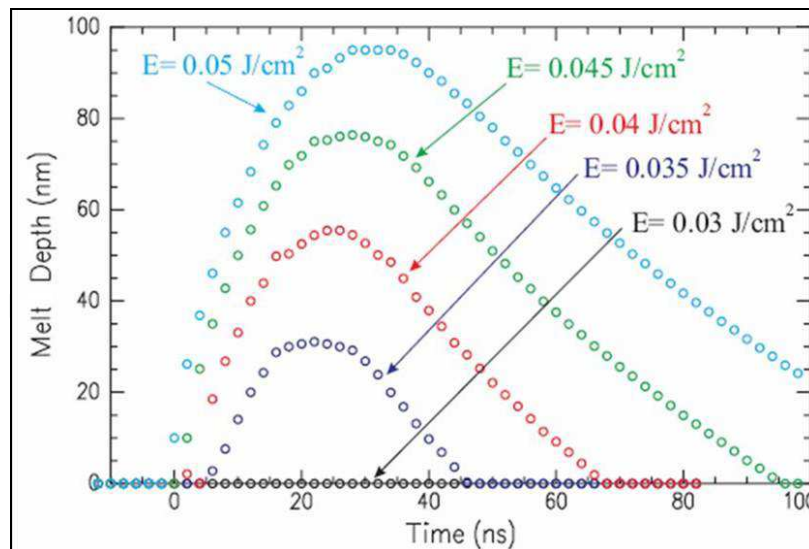
Fig. 4. Melted depth versus time as simulated for several energy densities.

Figure 5 shows the simulated melt depth as a function of laser energy density. The arrows indicate the energy density at which the thickness of melted material is expected to reach the film thickness of 70 nm. The simulated value of 40 mJ/cm² required to melt the entire film agrees very well with the energy density at which sheet resistance saturation is observed, indicating that all the material is converted into the amorphous phase by melt quenching.
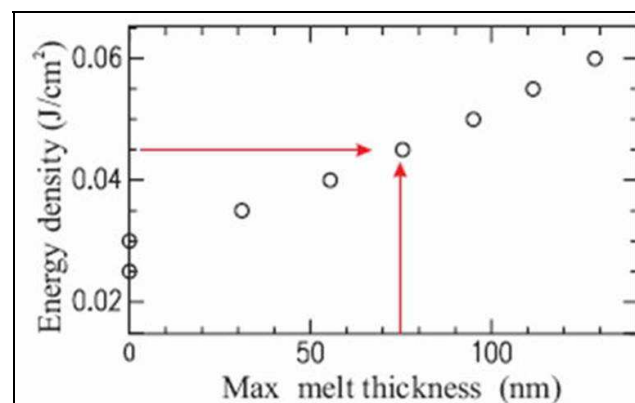

Fig. 5. Energy density versus melt thickness. For 70 nm thick film complete amorphization is expected above 40mJ/cm².

For comparison, amorphous films were also deposited at room temperature over SiO_2 covered Si substrates, from a single target by using RF sputter. Thickness of amorphous films was 50 nm. The stability of the amorphous resistance has been studied through sheet resistance measurements at different temperatures, in the range 40-120°C.

Figure 6 (a), (b) and (c) shows as black symbols the conductivity versus the reciprocal of temperature for as deposited, implanted and melt quenched amorphous films, respectively. The figure also shows as red symbols the conductivity obtained after annealing at temperatures below 140°C, i.e. not so high to produce the conversion into the crystalline phase. Four different samples have been measured for amorphous and as implanted

material. For melt quenching, samples irradiated at two different laser intensities have been tested. Both laser intensities values are high enough to melt and quench the entire film thickness.
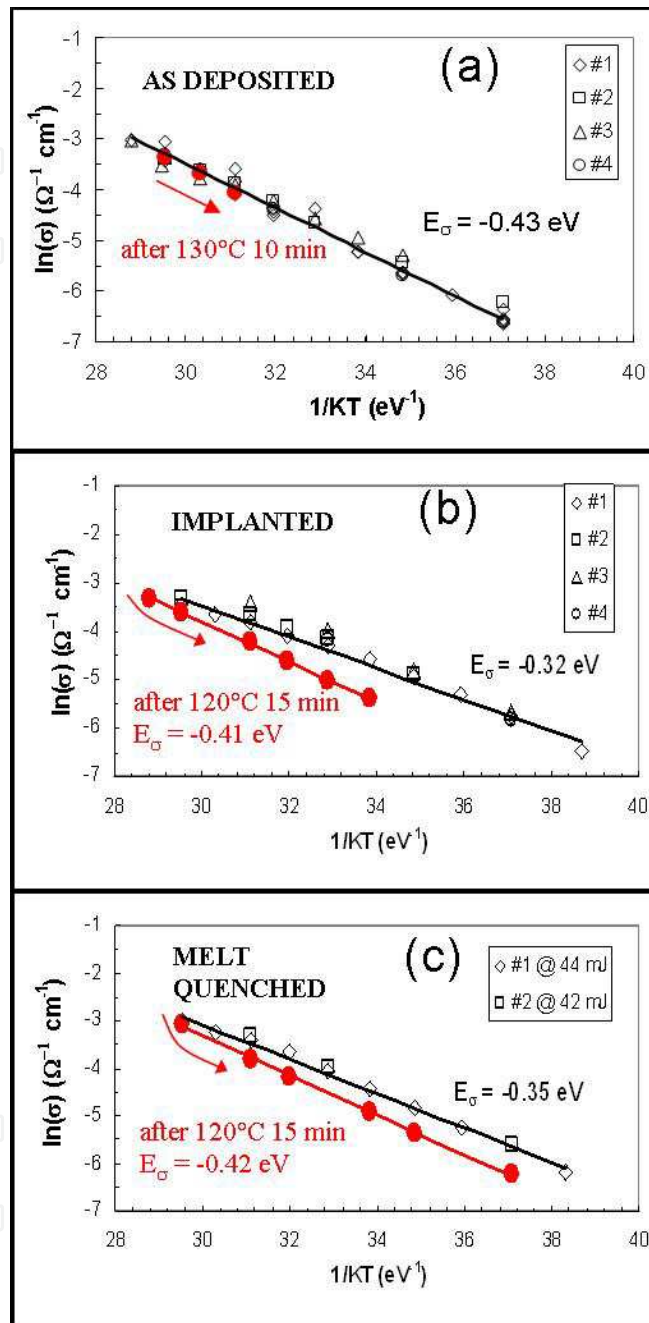

Fig. 6. Conductivity versus temperature for as deposited (a), implanted (b) and laser annealed (c) amorphous GST.

The carrier transport in amorphous GST in the temperature range we studied (40-120 °C), is dominated by the band conduction through extended states, in which the charge carriers hop between trap centers via excitations above the mobility edge. Therefore the conductivity of amorphous samples is exponentially dependent on the energy gap, whose value is about twice the activation energy for conduction (Mott & Davis, 1979).

In as deposited samples the mobility gap, measured by linearly fitting the data shown in Fig.6, is 0.86 eV and its value does not change after annealing at 130°C for 10 minutes. Therefore in as deposited GST we do not observe the resistance drift reported for PCM devices.

In films amorphized by ion implantation, instead, the conductivity decreases after annealing at 120°C. The mobility gap also changes from 0.7eV, obtained in fresh samples, to 0.82-0.84 eV, a value very close to the as deposited amorphous. A similar behavior is also observed for melt quenched amorphous films.

The drift of activation energy for conduction in amorphous GST has been already observed in amorphous cells and it has been explained considering two possible candidates: a change of the bandgap value due to mechanical strain; a change of the donor acceptor-like defect density (Pirovano et al., 2004). Under compressive strain the bandgap of several chalcogenide materials decreases by as much as 2eV/ relative volume variation (Kastner, 1972). It is known that the phase change cause a compression of 6%. Therefore melt-quenched films could exhibit lower bandgap due to accumulated mechanical stress. This stress can be then released, producing and increase of E_σ, thanks to the bandgap increase during stress release.

On the other hand, it has been observed that ion implantation can produce densification in phase change materials (Rimini et al., 2009), obtaining amorphous films of substantially higher mass density than as deposited amorphous films (Raoux et al., 2010). Therefore we can reasonably consider the observed modification of E_σ in both melt quenched and ion implanted film as due to compressive stress release.

Another possible explanation is given by recent calculations (Akola et al., 2010) and involves the role of Ge atoms bonding. Atomistic simulations of molecular dynamics performed on amorphous phase-change materials have shown that in melt quenched and as deposited amorphous GST, Germanium atoms have different environments: predominantly tetrahedral in as deposited GST and distorted octahedral in melt quenched. EXAFS data (Kolobov et al., 2004) indicate that in amorphous GST Ge atoms are prevalently tetrahedrally coordinated, with considerably shorter bond lengths (2.61-2.63 Å) than in the crystal, where Ge atoms occupy the octahedral position with Ge-Te bond length 2.83 Å. Therefore the decrease of activation energy for conduction observed in films amorphized by ion implantation and in melt quenched GST could be determined by a larger fraction of Ge atoms with distorted octahedral coordination.

4. Doping by Ion beam: Amorphous properties

Films doped with nitrogen, oxygen or fluorine have been obtained by ion implantation on amorphous $Ge_2Sb_2Te_5$. The energy of the ions was 15 keV, in order to have distributions peaked at the center of the film. Different fluencies were implanted, obtaining peak concentrations of 1.5 at.% and 10 at.% of nitrogen; 1.5 at.% and 6 at.% of oxygen; 1.5 at.% and 6 at.% of fluorine.

The amorphous properties were studied by electrical measurements. The sheet resistance was measured *in situ* using a four-point probe configuration, with the employment of a thermal chuck.
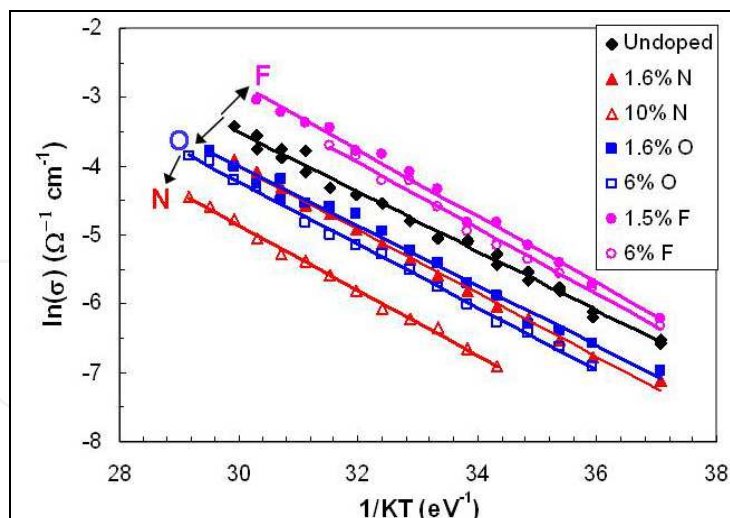
Fig. 7. Conductivity versus reciprocal temperature for undoped amorphous GST (diamonds) and samples doped with oxygen (squares), nitrogen (triangles) or fluorine (circles).

Figure 7 shows the conductivity of amorphous samples as a function of the reciprocal temperature, measured in undoped GST (black diamonds) and in samples with: 1.5 at.% of O (full squares), 6 at.% of O (open squares), 1.5 at.% of N (full triangles) 10 at.% of N (open triangles), 1.5 at.% of F (full circles) and 6 at.% of F (open circles). As shown by the arrows in Fig.7, in the case of nitrogen or oxygen doping, the conductivity decreases as the dopant concentration increases. In the case of GST doped with fluorine, instead, the conductivity increases.
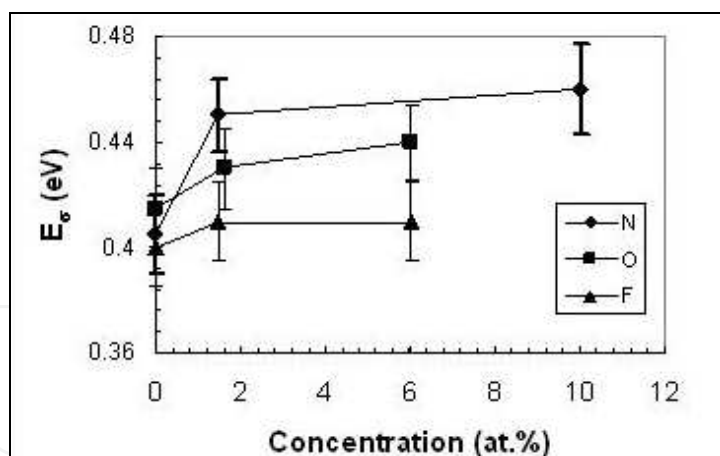

Fig. 8. Activation energy for conductivity as a function of doping concentration, obtained for nitrogen (diamonds), oxygen (squares) and fluorine (triangles).

Figure 8 shows the activation energy versus doping concentration, as obtained by linearly fitting data shown in Fig. 7.

In samples doped with nitrogen or oxygen the activation energy for conduction slightly increases, while for fluorine doping the activation energy remains almost the same. Largest variations have been obtained in the case of nitrogen: by doping GST with 10 at.% of N, the conductivity decreases of one order of magnitude and E_σ increases from 0.42 ± 0.01 eV, measured in undoped samples, up to 0.47 ± 0.01 eV.

These results are in agreement with changes in the optical band gaps of nitrogen doped GST films reported in literature (Kim et al., 2007), indicating that the increased band gap is closely related to the incorporation of nitrogen.

According to the results of numerical calculations shown by (Akola et al., 2010), an increased activation energy for conduction in nitrogen and oxygen doped samples could indicate the presence of more Ge atoms tetrahedrally coordinated.

5. Amorphous-to-crystal transition in undoped $Ge_2Sb_2Te_5$ films

Several experimental techniques have been employed to follow the amorphous-to-*fcc* transition in $Ge_2b_2Te_5$, such as optical or electrical measurements. However, only microscopical techniques allow to separate the contribution of nucleation and growth, obtaining valuable information for understanding of the involved physical mechanisms. For this reason we have studied by *in situ* transmission electron microscopy (TEM) the amorphous to crystal phase transition as a function of temperature and annealing time, obtaining a detailed measurement of all the physical parameters governing the transformation.

To render the sample transparent for TEM, specimens were ground, dimpled and etched in a HNO_3:HF:H_2O (4:1:1) solution. This procedure has been adopted because it assures no variation of the initial interfaces and film thickness, which could affect the nucleation and growth process (Ohshima, 1996, Friedrich et al., 2000). Indeed, the specimen under observation in the microscope does not contain a hole, but it is made by a continuous film over its SiO_2 substrate layer. Moreover, sample preparation by etching instead of conventional ion milling, can assures no undesired heating of the sample above the crystallization temperature, which could produce some pre-existing crystalline grains, therefore altering the kinetics of crystallization.

In situ TEM analyses have been performed using a JEOL 2010 TEM operating at 200 kV, with a sample holder equipped with a furnace around the specimen and a thermocouple. A magnification of 10000x was used for all the experiments. Since it has been shown the crystallization can be affected by the electron beam (Kooi et al., 2004), the beam has been switched off during annealing and fresh areas have been analysed, for each time step, in order to have a good statistical evaluation of the grain density and size. The transformation has been followed in the range of temperatures 130-143 °C.

Figure 9 (a) and (b) shows a TEM micrograph obtained for undoped GST after annealing at 135 °C for 50 min and 66 min, respectively. Grains appear as dark or bright circular regions and can be observed during the incubation regime (a), and after the onset of steady state nucleation (b). Grains with minimum detectable size of 7 nm are detected up to the complete crystallization, indicating that no saturation of nucleation sites occurs.

Figure 10 (a), (b), and (c) show the grain size distributions (GSDs) of samples annealed for various times, at 130 °C, 135°C and 140°C, respectively. GSDs have been obtained by assigning at each grain with surface area A an average radius $r = \sqrt{(A/\pi)}$, and by plotting, as a function of r, the density dN of crystalline grains with radius in the size interval $(r, r+dr)$, divided by dr. Figure 10 shows that all of the measured distributions smoothly decrease as a function of grain radius. At low grain size the distributions tend to reach the same value,

independent on time. This value indicates the establishment of steady state nucleation condition at the lowest grain radii. Moreover, the largest detected grain size increases with time, following a linear law.
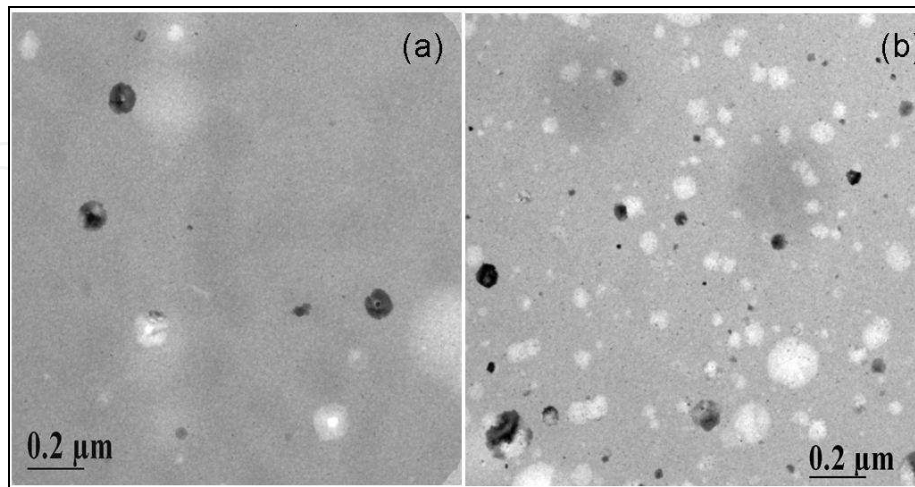

Fig. 9. TEM image of undoped amorphous GST after anneling at 135°C for 50 min (a) and 66 min (b).

From TEM images acquired at different annealing time, for several analyzed temperatures, it is possible to evaluate the evolution of the grain density ad the grain size distribution.
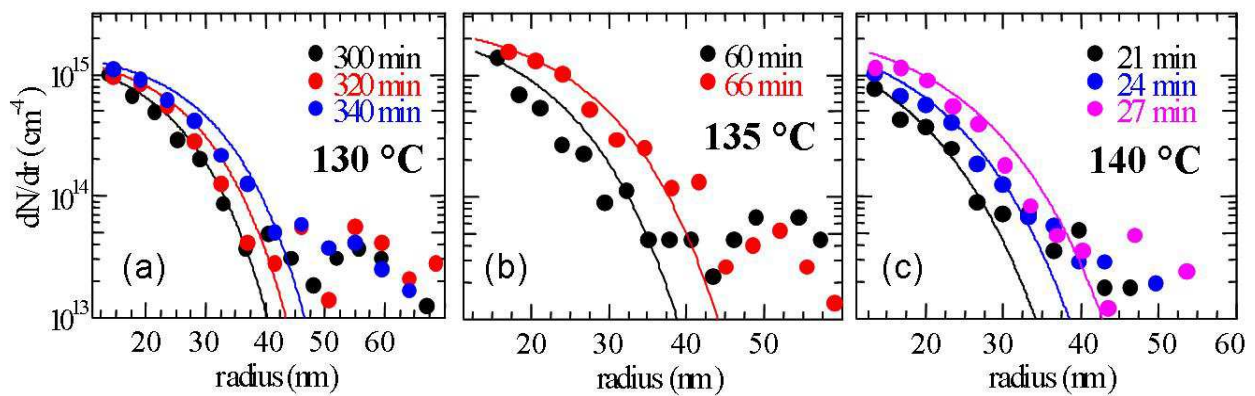

Fig. 10. Grain size distributions in undoped amorphous GST obtained after anneling at 130° C (a), 135°C (b) and 140°C (c). The distribution for each annealing temperature, have been obtained at different annealing time. Solid lines are fit to data.

According to a well known approach based on the capillarity approximation, the growth or shrinkage of a cluster is due to the attachment or detachment of atoms at the interface between the two phases. Assuming the transition is limited by the reaction at the interface, the net growth rate of individual nuclei can be approximated to (Turnbull &. Fisher, 1949):

$$v(r) = a\,f\,\varDelta g_v/(KT)\,(1-r^*/r) \tag{3}$$

where $r^* = 2\,a\,\gamma/\varDelta g_v$ is the critical radius, a is the lattice parameter, γ is the surface free energy at the interface, $\varDelta g_v$ is the free energy difference between the two phases per atom, $f = f_0\,exp[E_g/(KT)]$ is the thermally activated atomic jump frequency, and E_g is the activation

energy for the atomic motion responsible for the single elementary crystallization step. Therefore, for grain size much larger than r^*, $v(r)$ tends to $v_g = a\,f\,\Delta g_v/(KT)$.

The nucleation process at any time t for a given cluster size i can be in general described considering the nucleation rate $J_{i,t}$ of clusters with size larger than i.

It can be shown that the steady-state value of the nucleation rate (Becker & Döring, 1935) is:

$$J_{ss}=N_a\,O_{i^*}\,f\,[\Delta\,g_v\,/\,(6\,\pi KT\,i^*\,)]^{1/2}\,exp[\,-\Delta G^*\,/\,(KT)] \qquad (4)$$

where N_a is the atomic density and $O_{i^*} = 4\pi\,[3/(4\pi)]^{2/3}\,i^{*\,2/3}$ is the number of atoms at the surface of a critical nucleus. Following this description, the steady-state nucleation rate J_{ss} exhibits an activated temperature dependence with an activation energy $E_n=E_g + \Delta G^*$.

The steady-state condition does not exist from the beginning of the transformation but it is established after a transient period during which the nucleation rate depends on size and time. All the data acquired from *in situ* TEM analyses as a function of annealing time and temperature, i.e. the grain size distributions, the transformed fraction and the grain density, have been simultaneously fitted following the model proposed by (Shneidman, 1987, 1988, 1991), as described in detail in (Privitera et al., 2007a). Four main parameters are used for the fitting procedure, the nucleation rate, the growth rate, the incubation time and the transient time τ, representing the time spent by the growing cluster in the critical region. Results of fitting have been shown in fig. 10 as solid lines.

The main parameters determined by fitting, i.e. the nucleation rate and the growth velocity, exhibit an activated temperature dependence, with activation energy of 2.6 eV and 2.3 eV, respectively (Privitera et al., 2007a).

In the classical theory of nucleation, the difference between the activation energy for the nucleation rate and that for the growth velocity is equal to the barrier energy for the nucleation ΔG^*, which corresponds to the energy necessary for the nucleation of a critical nucleus. Following this description, the value of ΔG^* here determined is less than 1eV and can be explained by considering the effect of heterogeneous nucleation. In this case, the model is also valid, provided that the atomic density N_a is replaced by the density of nucleation sites and the barrier energy ΔG^* is reduced according to the lower surface energy term. Indeed, it has been observed that the nucleation of the metastable *fcc* phase is dependent on the substrate type and different activation energies have been found for $Ge_2Sb_2Te_5$ over different substrates (Ohshima, 1996, Friedrich et al., 2000). To clarify this point in-situ isothermal annealing experiments of cross-sectional scanning-TEM (STEM) specimens of GST have been also performed (Lombardo et al. 2010). This analysis has shown the formation of crystalline grains preferentially occurs near the upper free interface, subsequently followed by the nucleation of crystal grain also at the GST / SiO_2 interface.

By fitting the experimental data the pre-exponential terms can be also determined. Estimates of these can be done according to Eqs. (3) and (4) considering that f_0 is of the order of 10^{13} s^{-1}, the lattice parameter a and the GST density N_a are known, and the critical radius r^* can be evaluated as the product of the measured v_g at large sizes, multiplied by the transient time τ. Exponential factors for J_{ss}, v_g obtained from best fit to data, however, result anomalously different from the above estimates. In order to reproduce the experimental value of v_g, the

calculated value from Eq (3) should be multiplied by an adimensional factor equal to $\approx 7 \times 10^{13}$. For the steady-state nucleation rate J_{ss} we have to consider an additional factor equal to 0.3 which, however, is reasonably explained by the evidence of heterogeneous nucleation. So, data can be well explained by employing the classical model of grain growth and nucleation based on capillarity, provided that we consistently assume an anomalously large ($\approx 10^{14}$ times) factor multiplying the frequency of crystallization jumps.

This result has been extensively explained in (Privitera et al., 2007a) by considering the effect of maximum entropy production rate, based on the large disorder of the *fcc* crystal structure. The role of entropy in the grain growth during first order phase transformations has been put in clear evidence in literature (Hill, 1990), for example driving the transition from planar to dendritic growth. It is reasonable to expect that in our case the entropy production rate is extremely large. In fact, it has been shown that the *fcc* structure of GST is a combination of two *fcc* lattices, one made of Te atoms and a second made of Ge, Sb, and vacancies, in the ratio 2:2:1 (Yamada et al., 1991). The Ge:Sb:vacancy *fcc* sublattice is randomly occupied by the three species. Kolobov et al. (Kolobov et al., 2004) have proposed a crystalline structure made by short-range ordered building blocks that may rotate by 90 degrees in an arbitrary direction, giving rise to a random distribution of Ge, Sb and vacancies on a long-range scale. Based on the type of bonding experimentally observed by EXAFS in amorphous and *fcc* phases, they have also proposed that the amorphous to *fcc* transition is likely due to an atomic flip of the Ge, which jumps from sp³ tetrahedral bonds with four Te atoms, to an octahedral configuration, again surrounded by Te first neighbors (eight) but with bonds of a prevalent p character. Kolobov proposes that the memory principle is based on this Ge flipping effect (from tetrahedral to octahedral). Since it involves at the ultimate level a single Ge atom and its immediate neighbors, this mechanism does possess a very large potential for memory scaling. However, this only effect, cannot explain the observed high transition rate, coupled with the high activation energy. What we have proposed is that the anomalous pre-exponential factors experimentally observed can be explained in terms of Ge flipping, but taking into account also the large configuration entropy of the *fcc* crystal.

Indeed, as a consequence of a Ge flip, it follows that the number of atoms crystallized in a single flip event is much larger than one. Referring to Fig. 5 in (Kolobov et al., 2004) this is at least equal to 6 Te atoms plus their first neighbors Ge, Sb, or vacancy. These amount to a total of about 18 atoms and vacancies crystallized for a single Ge flip. The Ge:Sb:vacancy *fcc* sublattice contains 11 positions, randomly occupied either by Sb atoms or by vacancies. Therefore it has a large number of different possible configurations. A rough estimate can be done considering that we have 11 allowed positions that can be occupied by either a vacancy or a Sb atom, each one with 4 different possible positions (Kolobov et al., 2004). This means that the total number of possible configurations is of the order of $8^{11} \approx 8.6 \times 10^9$.

So, according to (Hill, 1990) that has shown that the entropy generation rate is proportional to the growth velocity and that the growth mode in a phase transition follows the criterion of maximum entropy generation rate, the effective frequency of crystallization jumps should be multiplied by the factor $18 \times 8^{11} \approx 1.5 \times 10^{11}$, taking into account for the number of crystallized atoms per Ge flip (≈ 18) and for the configuration entropy term ($\approx 8^{11}$).

This estimate does not reach the experimentally found factor (1.5×10^{11} against 7×10^{13}) but it represents a lower limit, found assuming one single Ge flip, no effect of Sb, and that no other Ge neighbor is in the *fcc* crystal phase. If we consider the configuration entropy contribution due to the presence of the pre-existing amorphous / crystal interface, the estimate of the pre-exponential factor would be larger, so we believe that the estimate presented, strictly based on a single Ge flip, is satisfactorily close to the experimental result.

The discussion here presented can be considered a starting point, from which it is clearly necessary to further investigate and find other evidences in favor. In agreement with the proposed description, it has been observed that the crystallization speed is increased in GeTe-Sb$_2$Te$_3$ compounds by partially replacing Sb atoms with Bi atoms (Matsunaga & Yamada, 2004), or when a proportion of Ge is replaced by Sn (Kojima & Yamada, 2001). Since both Sn and Bi occupy the same (4b) position as Ge and Sb in the *fcc* lattice (Matsunaga & Yamada, 2004), their presence definitely increases the number of possible configurations and therefore the entropy factor in the growth velocity.

Recently, the disorder of phase change materials has been also taken into account to explain metal-semiconductor transitions occurring in crystalline phase change GeSbTe alloy (Siegrist et al., 2011). The strong disorder, usually associated only with amorphous solids, seems to be at the origin of the remarkable reproducibility of the resistance switching observed in phase change material and strongly suggests that the disorder could be one of the key ingredient that makes the physical properties of phase change materials so peculiar.

6. Amorphous to crystal transition in doped films

Once we have studied in detail the crystallization process in undoped materials, we have investigated the effect of doping with light atom on the amorphous-to-crystal transition. In order to evidence the modifications due to doping, we have plotted in Fig. 11 the sheet resistance measured after 12 minutes anneals as a function of annealing temperature.
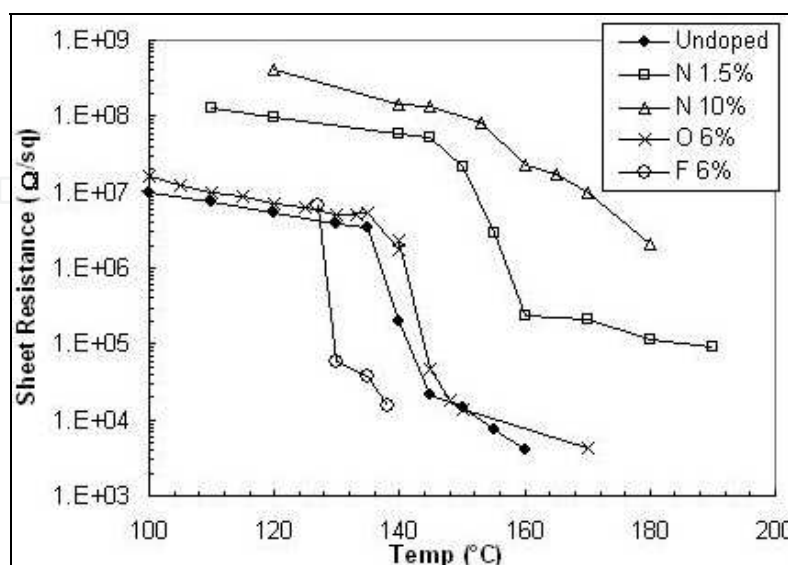

Fig. 11. Sheet resistance versus temperature as measured after 12 min isothermal anneals, for undoped and doped GST with oxygen (crosses), nitrogen (squares and triangles) or fluorine (circles).

Samples doped with nitrogen exhibit higher resistance in the amorphous phase and the crystallization occurs at much higher temperatures than undoped material. A small increase in the crystallization temperature is also observed by oxygen doping while, on the contrary, addition of fluorine produces a decrease in the crystallization temperature.

The dependence of the resistance as a function of time during isothermal anneals has been also studied by *in situ* resistance measurements using a four point probe. Figure 12 (a) and (b) shows the sheet resistance vs time as obtained during isothermal treatments at several annealing temperatures in the range 127-190°C, for undoped GST and for film doped by 6 at.% of fluorine, respectively. Fluorine doped samples are characterized by fast crystallization.
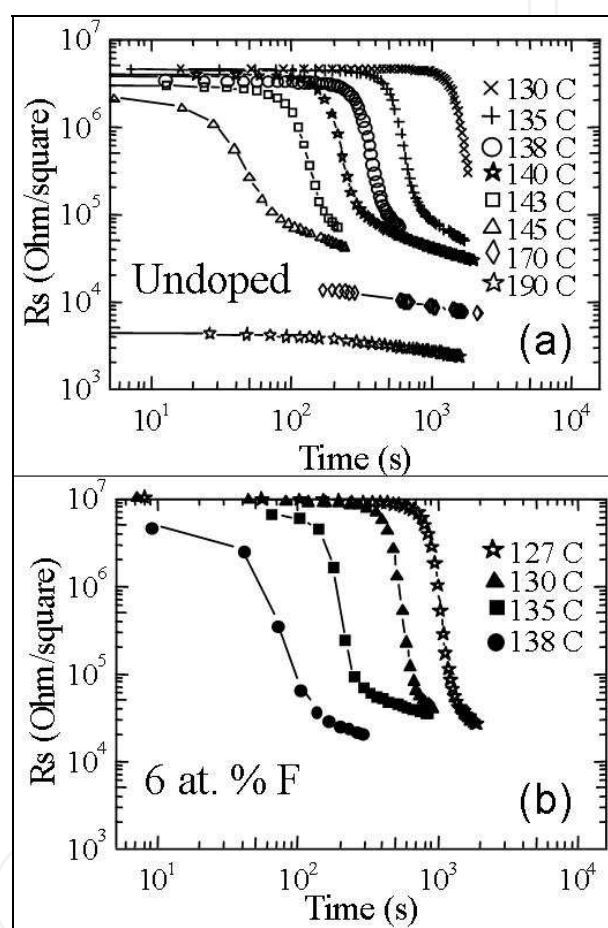

Fig. 12. Sheet resistance versus time as measured during anneal at various temperatures in the range 127-190°C, for undoped (a) and fluorine doped GST (b).

By taking the first derivative of the resistance versus time, the characteristic time for transition can be measured, as the time at which a minimum in the derivative is observed. The characteristic time has been then measured for all the studied samples and it has been used to determine the temperature dependence of the transformation. The activation energy obtained for undoped Ge$_2$Sb$_2$Te$_5$ is around 3 eV. The same value, within experimental errors, has been also determined for samples with low concentration of nitrogen and fluorine, as shown in Figure 13, reprinted from (Privitera et al. 2007b). Higher activation energy has been instead measured in GST doped with 6 at. % of oxygen.

Characteristic times observed in N and O doped samples are up to one order of magnitude higher than in pure GST, whilst the characteristic times observed in fluorine doped samples are lower.
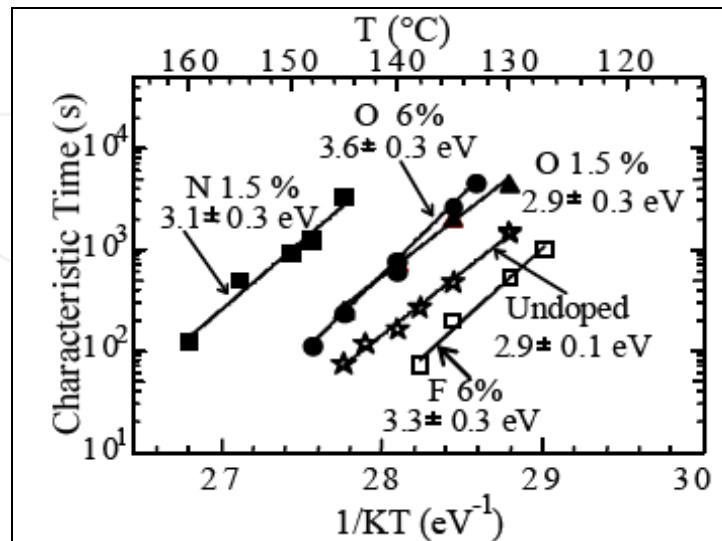

Fig. 13. Activation energy for crystallization in Undoped and Doped GST with O, N, or F. Reprinted from (Privitera et al., 2007b)

Results from electrical measurements have been related to the kinetics of the transformation through *in situ* TEM analyses. Figure 14 shows typical TEM plan view images obtained during the amorphous-to-*fcc* transition in different samples annealed at 130°C. Fig. 14 (a) has been acquired for undoped sample annealed at 130°C for 240 min. A few crystalline grains embedded in the amorphous matrix are visible as dark or bright regions. Fig. 14 (b) shows a sample doped by 6 at.% of oxygen, annealed at the same temperature and time of 130°C 240 min. The material is almost completely amorphous and only small crystalline grains can be detected. Such a result is a confirmation of the observed increase of incubation and characteristic times observed by electrical measurements, as shown in figures 12 and 13.
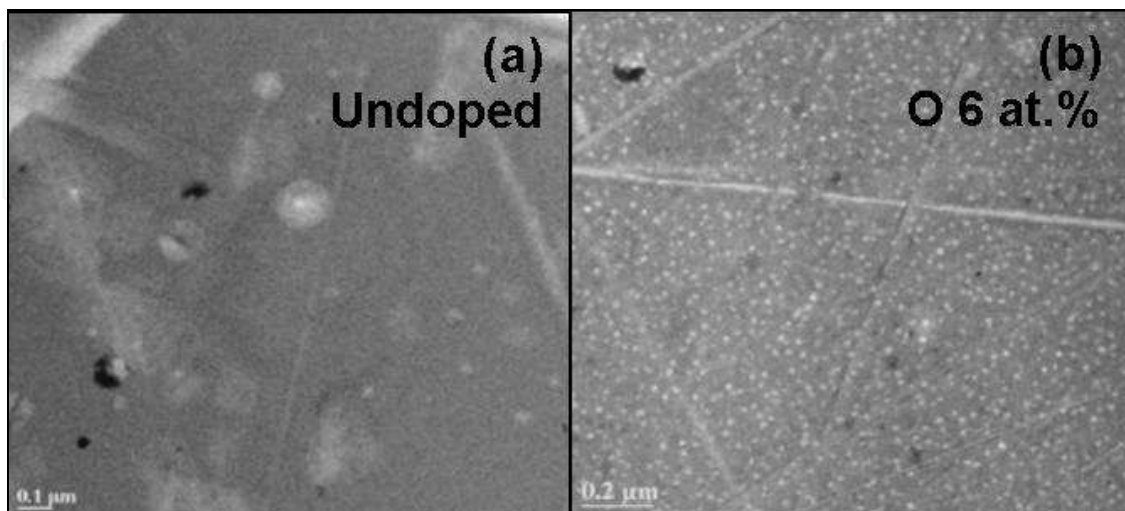

Fig. 14. Comparison between TEM image of amorphous GST after anneling at 130°C for 240 min for undoped (a) and oxygen doped GST (6at.%) (b).

Under annealing at higher temperature, samples doped with oxygen exhibit higher crystallization rate, compared to undoped GST. Figure 15 (a) and (b) shows TEM images of samples annealed in situ at 137°C for undoped and 6 at.% oxygen doped GST, respectively. Figure 15 (a) has been obtained in undoped material after 107 min annealing, while the image shown in fig. 15 (b) has been acquired on oxygen doped sample after only 70 minutes. Although annealed for shorter time, doped sample exhibits higher grain density and larger grain size.
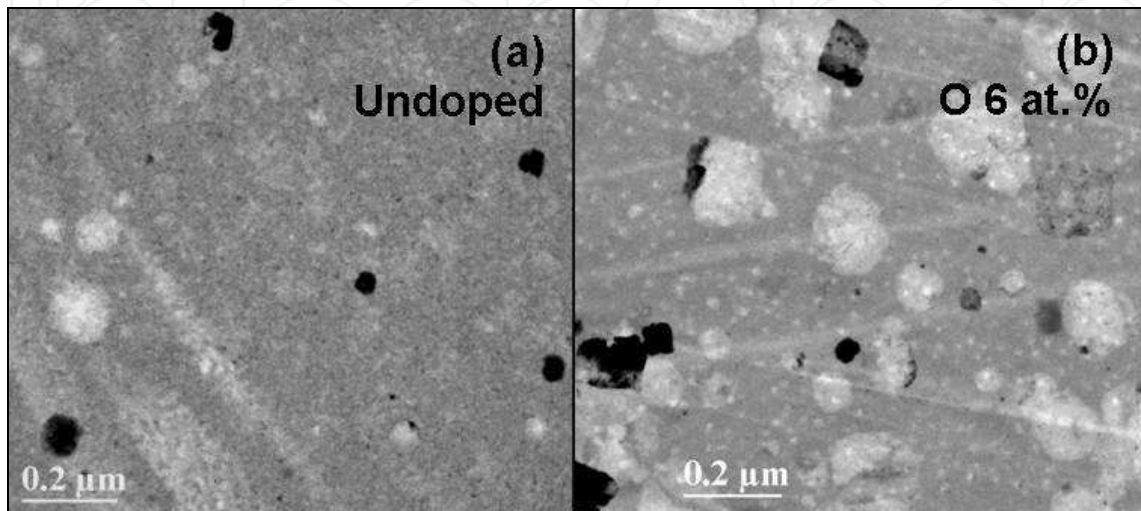

Fig. 15. TEM image of undoped amorphous GST after anneling at 137°C for 107 min (a) and of oxygen doped GST (6at.%) after annealing at 137°C for 70 min (b).

Such a results is in agreement with the higher activation energy obtained in O doped blanket material (Fig. 13) and in oxygen doped memory cells (Matsuzaki et al., 2005). Moreover, increase of the crystal grain size has been also reported in 6 at. % oxygen-doped phase change optical recording disk, improving the overwrite cyclability of the optical recording disk. Therefore, the increase of activation energy, coupled with the increase of incubation time, makes oxygen doped GST particularly interesting for cell endurance improvement, without decreasing the crystallization rate, i.e. without increasing the writing time.

The addition of 1.5 at.% of nitrogen by ion implantation produces strong variations in the kinetics of the transformation.

Figure 16 (a) and (b) shows the comparison between undoped sample (a) and sample with 1.5 at.% of N (b) after annealing at 140 °C for 75 min and 150 min, respectively. Nitrogen doped samples exhibit much longer incubation time compared to undoped film: after 150 min the material is still almost completely amorphous and only small crystallites are visible.

Even after annealing at higher temperature, the morphology of nitrogen doped films appears different from the one observed in undoped materials. As an example, Figure 17 shows a TEM image of a nitrogen doped sample (1.5 at.%) annealed at 150°C for 80 minutes. The film is crystalline but it is characterized by small crystalline size.

We have already observed in section 5 that the crystallization of undoped GST is heterogeneous and preferentially occurs near the upper free interface and, secondarily, at the GST / SiO$_2$ interface.
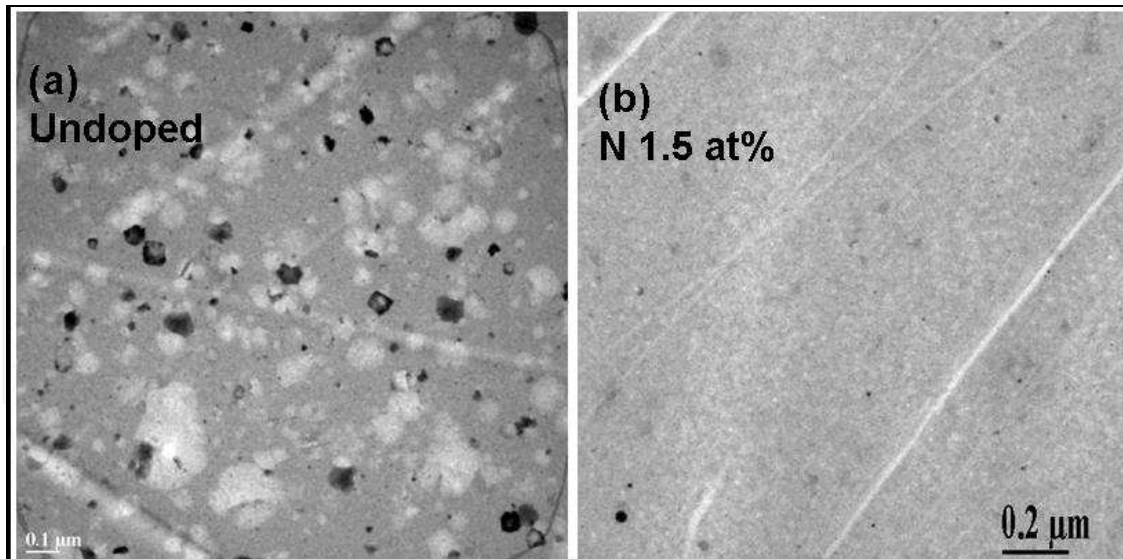
Fig. 16. TEM image of undoped amorphous GST after anneling at 140°C for 75 min (a) and of nitrogen doped GST (1.5 at.%) after annealing at 140°C for 150 min (b).

Since the ion implantation can modify the interfaces, causing some intermixing, we have performed in situ TEM analyses in cross section. Figure 18 (a) and (b) shows the amorphous GST film doped with 1.5 at.% of N as deposited and after annealing in situ at 150°C for 20 min, respectively. As observed for undoped GST (Lombardo et al., 2010) a continuous polycrystalline layer is formed. However, in contrast with observation on pure GST, in the case of nitrogen doping the nucleation has occurred preferentially at the GST/SiO$_2$ interface, with the addition of small dispersed crystalline regions in the amorphous material and at the upper interface. Therefore doping by ion implantation is also effective in modifying the nucleation sites at which heterogeneous nucleation preferentially occurs.
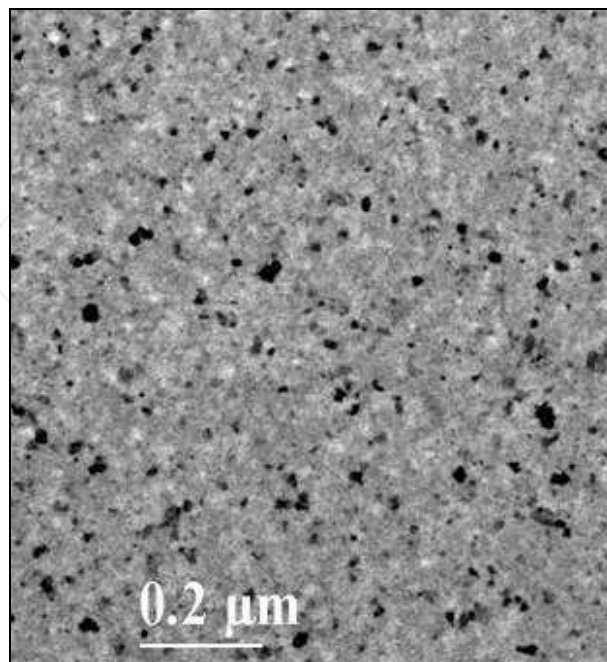

Fig. 17. TEM image of a sample doped by 1.5at.%of nitrogen annealed at 150°C for 80 min.
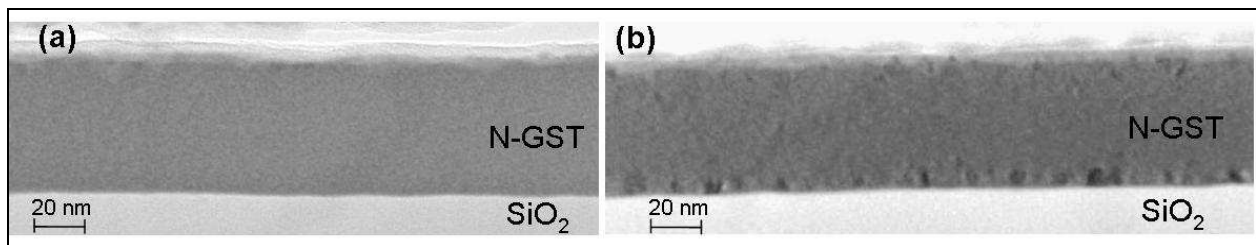
Fig. 18. Bright field TEM micrographs in cross section of a sample doped by N 1.5 at.% as-deposited (a), and annealed in situ at 150°C for 20 min (b). The first crystalline formation is clearly visible at the GST/SiO₂ interface, with additional crystalline grains nucleated also at the upper interface.

Therefore it appears clear from the experimental data that, at least in the range of compositions here investigated, the oxygen or nitrogen doping affects the crystallization process differently, the first one producing higher crystallization rate and larger grain size, while N doping gives rise to grain size refinement and longer incubation time.

The increase of the crystallization temperature in oxygen (Jeong et al., 2001) and nitrogen [Kojima et al., 1998, Jeong et al., 2000) doped GST has been already reported in literature, as well as the reduction of the grain size in samples containing nitrogen. Several models have been proposed (Jeong et al., 2001, Jeong et al., 2000) trying to simultaneously explaining the effect of both O and N in order to find the optimal dopant to engineer specific properties of GST.

First, it has been observed that the reduced grain size could be caused by dopant segregation near grain boundaries in the form of nitrides (Kojima et al., 1998). The resistance of the crystalline phase would increase due to additional electron scattering from grain boundaries (Horii et al., 2003). We cannot exclude, in the samples with 10 at.% of N, the formation of very thin nitrides layers at grain boundaries, which are probably responsible for the increased resistivity of the crystalline phase and for the smoothing of the shape of the resistance versus temperature shown in Fig. 11.

Regarding oxygen doping, the formation of Ge or Sb oxides has been reported for concentrations above 10 at.% (Jang et al., 2009, Morales-Sanchez et al., 2006). For lower concentration, as in the samples we have studied, no oxidation seems to occur. It has been therefore proposed that oxygen atoms, as well as nitrogen atoms at low concentration, are located at the tetrahedral interstitial sites (Jeong et al., 2000). Indeed, since nitrogen and oxygen have quite small atomic sizes compared to that of Ge, Sb and Te, they cannot substitute these atoms, filling the vacancies which are present in the structure. Therefore their effect is expected to be very different from the one observed in the case of Bi or Sn, (Matsunaga & Yamada, 2004), which substituting in the Ge:Sb:vacancy lattice, can increase the number of possible configurations and therefore the growth velocity. N or O atoms will be instead located at the tetrahedral interstitial sites distorting the unit cell and resulting in a strain field (Jeong et al., 2000). Since nitrogen has a larger atomic radius (0.071 nm) (Lide, 2004), compared to oxygen (0.066 nm) (Lide, 2004), a larger amount of strain is expected to accommodate nitrogen atoms in the structure.

Another factor to be taken into account together with the stress is the chemical bond between Ge and Te and its modifications due to the presence of nitrogen, or other dopants.

The main crystallization mechanism has been identified as an atomic flip of the Ge, which jumps from tetrahedral bonds with 4 Te atoms, to an octahedral configuration, surrounded by 8 Te first neighbors. Xray photoemission spectroscopy (XPS) analyses by employing synchrotron radiation have shown that when a GST film is crystallized in the *fcc* structure, the intensity of Germanium in tetrahedral position is decreased while the intensity of Ge octahedral is increased owing to the umbrella-flip change in Ge atoms from the tetrahedral to the octahedral position (Kolobov et al., 2004).

Both experimental data (Kim et al., 2007, Jung et al., 2007) and atomic *ab initio* calculations (Cho et al., 2011) performed on nitrogen doped GST have shown that the N atoms are prevalently bonded with the Ge atoms to form GeN_x, rather than bonding with the Te or Sb atoms. Moreover, data of Ref. (Kim et al., 2007) show that the formation of Ge-N bonds can disturb the umbrella-flip of Ge atoms between the tetrahedral and octahedral positions because, as nitrogen is incorporated into the GST film, the intensity of the peak relative to Germanium in the octahedral position is decreased, since nitrogen combines with Ge to form germanium nitrides. By reducing the portion of the peak of Ge octahedral nitrogen is therefore effective in suppressing the crystallization.

A similar behavior is expected also for oxygen atoms, with the formation of Ge-O bonds. However, nitrogen can form three bonds while oxygen only two. Moreover, N dopants increase the portion of tetrahedral Ge atoms, while, on the base of calculations reported in (Cho et al., 2011), O doped GST seems to be more similar to undoped material, without favoring tetrahedral sites respect to octahedral Ge atoms. This could explain the lower increase in the energy gap observed in the case of oxygen (Fig. 8).

Considering the heterogeneous character of the transformation, the proposed assumption that oxygen and a small amount of germanium oxide could act as nucleation centers during crystallization, increasing the crystallization rate (Morales-Sanchez et al., 2006) could be a good explanation.

The decrease of crystallization temperature observed for fluorine doping remains to be better investigated. It has been reported that amorphous GST can have fast crystallization under compressive stress. So the effect of F could be explained with the introduction of compressive stress in the amorphous material. More extensive studies however are needed to map out the relationship between the chemical nature of dopants and the induced modifications in the phase change structure, in order to better identify the optimal dopant in order to achieve the desired properties.

7. Conclusions

In this chapter we reviewed some applications of ion beam to the study of the physical properties of $Ge_2Sb_2Te_5$, the phase change material most widely employed for application as nonvolatile memories. Phase change memories are one of the most promising solutions as replacement of current FLASH technology, based on charge storage, but some material properties need to be optimized. We have shown that ion implantation can be successfully employed to modify the properties of the amorphous phase change material, obtaining conduction properties very similar to those of melt-quenched amorphous material, formed by electric pulses or laser in memory cells.

Ion implantation can be also adopted for doping of phase change materials, modifying the amorphous-to-crystal transition kinetics, upon which the reliability definitely depends. The crystallization is a fast process occurring at very low temperature, compared to other solid materials. The explanation of such a fast transition has been found in the peculiar structure of the *fcc* phase which contains a large amount of disorder and whose formation is driven by flips of Ge atoms. By nitrogen implantation it is possible to increase the crystallization temperature and the crystalline resistance improving the cell endurance, reducing the RESET current and enabling the use of PCM also for high temperature applications, such as automotive. The formation of Ge-N bonds has been identified as the main effect determining the increase of crystallization temperature, the increase of the band gap in the amorphous material and the reduction of crystalline grain size.

By oxygen implantation, a moderate increase of crystallization temperature has been obtained, maintaining short crystallization time, thanks to the increased activation energy. Decrease of crystallization temperature has been instead obtained by fluorine doping. The way these doping acts is still not well understood and more extensive studies are required to relate the chemical nature of dopants belonging to different groups in the periodic table to the induced modifications in the phase change structure, in order to optimize the dopant specie on the base of the desired properties.

8. Acknowledgment

## 9. References

Akola, J.; Larrucea, J. & Jones, R. O. (2010), Polymorphism in amorphous Ge$_2$Sb$_2$Te$_5$: comparison of melt-quenched and as-deposited structures, *EPCOS 2010*, Milano, Italy, 2010. Available from
http://www.epcos.org/library/papers/pdf_2010/Oral/F03-Akola.pdf

B.-S. Lee, G. W. Burr, R. M. Shelby, S. Raoux, C. T. Rettner, S. N. Bogle, K. Darmawikarta, S. G. Bishop, and J. R. Abelson, Direct observation of the role of subcritical nuclei in crystallization of a glassy solid, *Science,* Vol. 326, No. 5955, (November 2009), pp. 980-984, ISSN 0036-8075.

Baeri, P. & Campisano, S.U. (1982) Chapter 4: Heat Flow Calculations, In: *Laser Annealing of Semiconductors,* ed. by J. M. Poate & J. W. Mayer, pp. 75-110, Academic Press, ISBN 0125588208, New York.

Becker, R. & Döring, W. (1935) Kinetische behandlung der keimbildung in übersättigten dämpfen, *Annalen der Physik* (Leipzig), Vol. 24, N. 8 (1935), pp.719-752, ISSN 00033804.

Boniardi, M.; Redaelli, A.; Pirovano, A.; Tortorelli, I.; Ielmini, D.; & Pellizzer, F. (2009). A physics-based model of electrical conduction decrease with time in amorphous Ge$_2$Sb$_2$Te$_5$, *Journal of Applied Physics,* Vol. 105, No. 8, (April 2009), pp. 084506-084506-5, ISSN 0021-8979.

De Bastiani, R.; Piro, A. M.; Grimaldi, M. G.; Rimini, E.; Baratta, G. A. & Strazzulla, G. (2008). Ion irradiation induced local structural changes in amorphous Ge$_2$Sb$_2$Te$_5$ thin films, *Applied Physics Letters*, Vol. 92, No. 24 (June 2008), pp. 241925- 241925-3, ISSN 0003-6951.

Friedrich, I.; Weidenhof, V.; Njoroge, W.; Franz, P. & Wuttig, M. (2000), Structural transformations of Ge$_2$Sb$_2$Te$_5$ films studied by electrical resistance measurements, *Journal of Applied Physics,* Vol.87, No. 9, (May 2000), pp. 4130 -4134, ISSN 0021-8979.

 Hill, A. (1990) Entropy production as the selection rule between different growth morphologies, *Nature*, Vol. 348, N. 6300 (November 1990) pp. 426-427. ISSN 0028-0836

Horii, H.; Yi, J.H.; Park, J.H.; Ha, Y.H.; Baek, I.G.; Park, S.O.; Hwang, Y.N.; Lee, S.H.; Kim, Y.T.; Lee, K.H.; U-In Chung; & Moon, J.T. (2003) A novel cell technology using N-doped GeSbTe films for phase change RAM, *2003 Symposium on VLSI Technology. Digest of Technical Papers,* pp.177-178, ISBN 4-89114-033-X, Kyoto, Japan, 10-12 June, 2003

Ielmini, D. (2008). Threshold switching mechanism by high-field energy gain in the hopping transport of chalcogenide glasses, *Physical Review B*, Vol. 78, No. 3 (July 2008), pp. 035308-035308-8, ISSN 1098-0121.

Im, J.; Cho, E.; Kim, D.; Horii, H,.; Ihm, J. & Han, S. (2010) Effects of pressure on atomic and electronic structure and crystallization dynamics of amorphous Ge$_2$Sb$_2$Te$_5$, Physical Review B, Vol. 81, No. 24, (June 2010), pp. 245211-245211-5, ISSN 1098-0121

Jang, M. H.; Park, S. J.; Lim, D. H.; Cho, M.-H.; Do, K. H.; Ko, D.-H. & Sohn, H. C. (2009) Phase change behavior in oxygen-incorporated Ge$_2$Sb$_2$Te$_5$ films, *Applied Physics Letters*, Vol. 95, No. 1 (January 2009), pp. 012102-012102-3, ISSN 0003-6951.

Jeong, T. H.; Kim, M. R. ; Seo, H. ; Park, J. W. & Yeon, C. (2000). Investigation of Crystallization Behavior of Sputter-Deposited Nitrogen-Doped Amorphous Ge$_2$Sb$_2$Te$_5$ Thin Films, *Japanese Journal of Applied Physics,* Vol. 39, No. 5A, (May 2000), pp. 2775-2779, ISSN 1347-4065.

Jeong, T. H.; Seo, H.; Lee, K. L. ; Choi, S. M.; Kim, S. J. ; & Kim, S. Y. (2001), Study of Oxygen-Doped GeSbTe Film and Its Effect as an Interface Layer on the Recording Properties in the Blue Wavelength, *Japanese Journal of Applied Physics,* Vol. 40, No. 3B, (March 2001), pp. 1609-1612, ISSN 1347-4065.

Jung, M.-C. Lee, Y. M. Kim, H.-D. Kim, M. G. Shin, H. J. Kim, K. H. Song, S. A. Jeong, H. S. Ko, C. H. Han, M. (2007) Ge nitride formation in N-doped amorphous Ge$_2$Sb$_2$Te$_5$, *Applied Physics Letters*, Vol. 91, No. 8 (August 2007), pp. 083514 - 083514-3, ISSN 0003-6951

Kastner, M. (1972). Compositional trends in the optical properties of amorphous lone-pair semiconductors, *Physical Review B*, Vol. 7, No. 12 (June 1973), pp. 5237-5252, ISSN 1098-0121.

Kim, Y.; Jeong, K.; Cho, M.-H.; Hwang, U.; Jeong, H. S. & Kim, K. (2007), Changes in the electronic structures and optical band gap of Ge$_2$Sb$_2$Te and N-doped Ge$_2$Sb$_2$Te during phase transition, *Applied Physics Letters*, Vol. 90, No. 17 (April 2007), pp. 171920-171920-3, ISSN 0003-6951.

Kojima, R. & Yamada, N. (2001), Acceleration of Crystallization Speed by Sn Addition to Ge–Sb–Te Phase-Change Recording Material, *Japanese Journal of Applied Physics*, Vol. 40 Part 1, No. 10, (October 2001) pp. 5930–5937, ISSN 1347-4065.

Kojima, R.; Okabayashi, S.; Kashihara, T.; Horai, K.; Matsunaga, T.; Ohno, E.; Yamada, N. & T. Ohta (1998) Nitrogen Doping Effect on Phase Change Optical Disks, *Japanese Journal of Applied Physics,* Vol.37, No. 4B, (April 1998), pp. 2098-2103, ISSN 1347-4065.

Kolobov, A. V.; Fons, P. ; Frenkel, A. I. ; Ankudinov, A. L. ; Tominaga, J. & Uruga, T. (2004) Understanding the phase-change mechanism of rewritable optical media, *Nature Materials,* Vol.3 (September 2004), pp.703-708, ISSN 1476-1122.

Kooi, B. J.; Groot, W. M. G. & De Hosson, J. Th. M. (2004) In situ transmission electron microscopy study of the crystallization of Ge$_2$Sb$_2$Te$_5$, *Journal of Applied Physics,* Vol.95, No. 3, (February 2004), pp. 924-932, ISSN 0021-8979.

Krebs, D.; Raoux, S. ; Rettner, C. T. ; Burr, G.W.; Salinga, M. & Wuttig, M. (2009). Threshold field of phase change memory materials measured using phase change bridge devices, *Applied Physics Letters*, Vol. 95, No. 8, (August 2009), pp. 082101-082101-3, ISSN 0003-6951.

Lai, S.; Lowrey, T., (2001). OUM-A 180nm Nonvolatile Memory Cell Element Technology for Stand Alone and Embedded Applications, *Electron Devices Meeting, 2001. IEDM Technical Digest. International,* pp. 36.5.1 - 36.5.4, ISBN 0-7803-7050-3, Washington, DC, USA, Dec 2-5, 2001

Lide, D. R. (2004) *CRC Handbook of Chemistry and Physics,* 85th Edition, CRC Press LLC, ISBN 0-8493-0485-7, Boca Raton, Florida, USA.

Lombardo S., Rimini, E.; Grimaldi, M.G. & Privitera, S. (2010) Amorphous-*fcc* transition in Ge$_2$Sb$_2$Te$_5$, *Microelectronic Engineering*, Vol.83, No.3, (March 2010), pp. 294-300, ISSN 0167-9317.

Matsunaga, T. & Yamada N. (2004) Crystallographic Studies on High-Speed Phase-Change Materials Used for Rewritable Optical Recording Disks, *Japanese Journal of Applied Physics,* Vol. 43, No. 7B, (July 2004), pp. 4704–4712, ISSN 1347-4065.

Matsuzaki, N.; Kurotsuchi, K.; Matsui, Y.; Tonomura, O.; Yamamoto, N.; Fujisaki, Y.; Kitai, N.; Takemura, R.; Osada, K.; Hanzawa, S.; Moriya, H.; Iwasaki, T.; Kawahara, T.; Takaura, N.; Terao, M.; Matsuoka, M. & Moniwa, M. (2005), Oxygen-doped GeSbTe phase-change memory cells featuring 1.5-V/100-μA standard 0.13μm CMOS operations, *Electron Devices Meeting, 2005. IEDM Technical Digest. International,* pp. 738 - 741, ISBN 0-7803-9268-X, Washington, DC, USA, Dec 5-7, 2005

Mio, A. M.; Carria, E. ; De Bastiani, R.; Miritello, M. ; Bongiorno, C.; D'Arrigo, G.; Spinella, C.; Grimaldi, M. G. & Rimini, E. (2010). Crystallization of ion amorphized Ge$_2$Sb$_2$Te$_5$ in nano-structured thin films, *Proceedings of Materials Research Society*, pp. 1251-H02-03, ISSN 0272-9172 , San Francisco, CA, USA, April 5-9, 2010.

Morales-Sanchez, E.; Gonzalez-Hernandez, J.; Herrera-Fierro, P.; Chao, B.; Kovalenko, Yu. & Prokhorov, E. (2006) Influence of oxygen on the crystallization process in Ge: Sb:Te:O films, 3rd International Conference on Electrical and Electronics Engineering, 2006, pp. 1-4, ISBN 1-4244-0402-9, Veracruz, Mexico, Sept 6-8, 2006.

Mott, N. F. & Davis, E. A. (1979) *Electronic processes in Non-Crystalline Materials,* Clarendon, ISBN 0198512880, Oxford.

Ohshima, N. (1996) , Crystallization of germanium–antimony–tellurium amorphous thin film sandwiched between various dielectric protective films, *Journal of Applied Physics,* Vol. 79, No. 11 (June 1996) , pp. 8357-8363, ISSN 0021-8979.

Owen, A. E.; Robertson, J. M. & Main, C. (1979). The threshold characteristics of chalcogenide-glass memory switches, *Journal of Non-Crystalline Solids*, Vol. 32, No. 1-3 (February-March 1979) pp. 29–52, ISSN 0022-3093.

Pirovano, A.; Lacaita, A.L.; Pellizzer, F.; Kostylev, S.A.; Benvenuti, A. & Bez, R. (2004). Low-field amorphous state resistance and threshold voltage drift in chalcogenide materials, *IEEE Transaction on Electron Devices*, vol. 51, No. 5, (May 2004), pp. 714–719, ISSN 0018-9383.

Privitera, S.; Lombardo, S.; Bongiorno, C.; Rimini, E. & Pirovano, A. (2007a). Phase change mechanisms in $Ge_2Sb_2Te_5$, *Journal of Applied Physics*, Vol. 102, No. 1 (July 2007) , pp. 013516 -1013516-5, ISSN 0021-8979.

Privitera, S.; Rimini, E. & Zonca, R. (2004), Amorphous-to-crystal transition of nitrogen- and oxygen-doped $Ge_2Sb_2Te_5$ films studied by in situ resistance measurements, *Applied Physics Letters*, Vol. 85, No. 15 (October 2004), pp. 3044-3046, ISSN 0003-6951.

Privitera, S.; Rimini, E.; Bongiorno, C.; Pirovano, A. & Bez, R. (2007b). Effects of dopants on the amorphous-to-fcc transition in $Ge_2Sb_2Te_5$ thin films, *Nuclear Instruments and Methods in Physics Research B*, Vol. 257, No. 1-2 (April 2007), pp. 352-354, ISSN 0168-583X.

Raoux, S.; Cohen, G. M.; Shelby, R. M.; Cheng, H.-Y. & Jordan-Sweet, J. L. (2010). Amorphization of crystalline phase change m aterial by ion implantation", *Proceedings of Materials Research Society*, pp. 1251-H02-06, ISSN 0272-9172, San Francisco, CA, USA, April 5-9, 2010.

Raoux, S.; Cohen, G. M.; Shelby, R. M.; Cheng, H.-Y.; Madan, A.; Ott, J. & Jordan Sweet, J. L. (2010). Effect of Ion Implantation on Crystallization Properties of Phase Change Materials, *EPCOS 2010*, Milano, Italy, 2010. Available from http://www.epcos.org/library/papers/pdf_2010/Oral/D01-Raoux.pdf

Redaelli, A.; Pirovano, A., (2011). Nano-scaled chalcogenide-based memories. *Nanotechnology*, Vol. 22, No. 25 (June 2011), pp. 254021-254025, ISSN 1361-6528.

Rimini, E.; De Bastiani, R. ; Carria, E. ; Grimaldi, M. G. ; Nicotra, G. ; Bongiorno, C. & Spinella, C. (2009). Crystallization of sputtered-deposited and ion implanted amorphous $Ge_2Sb_2Te_5$ thin films, *Journal of Applied Physics*, Vol. 105, No. 12 (June 2009) , pp. 123502-123502-6, ISSN 0021-8979.

Shneidman, V. A. (1987) Size-distribution of new-phase particles during transient condensation of a supercooled gas. *Soviet Physics Technical Physics*, Vol. 32, (1987), pp. 76-81, ISSN 0038-5662

Shneidman, V. A. (1988) Establishment of a steady-state nucleation regime. Theory and comparison with experimental data for glasses, *Soviet Physics Technical Physics*, Vol.33, (1988), pp.1338-1342, ISSN 0038-5662

Shneidman, V. A. (1991) Transient critical flux in nucleation theory, *Physical Review A* Vol.44, No.4 (August 1991), pp. 2609-2611, ISSN 1050-2947

Siegrist, T.; Jost, P.; Volker, H.; Woda, M. ; Merkelbach, P.; Schlockermann, C. & Wuttig M. (2011), Disorder-induced localization in crystalline phase-change materials, *Nature Materials*, Vol. 10, (January 2011), pp.208-210, ISSN 1476-1122.

Turnbull, S. & Fisher, J. C. (1949) Rate of nucleation in condensed systems, *Journal of Chemical Physics*, Vol. 17, No. 1 (January 1949), pp. 71-73, ISSN 0021-9606.

Yamada, N.; Ohno, E. ; Nishiuchi, K. ; Akahira, N. & Takao, M. (1991) Rapid-phase transitions of $GeTe$-Sb_2Te_3 pseudobinary amorphous thin films for an optical disk memory, *Journal of Applied Physics*, Vol. 69, No. 5, (March 1991), pp.2849 -2856 ISSN 0021-8979.
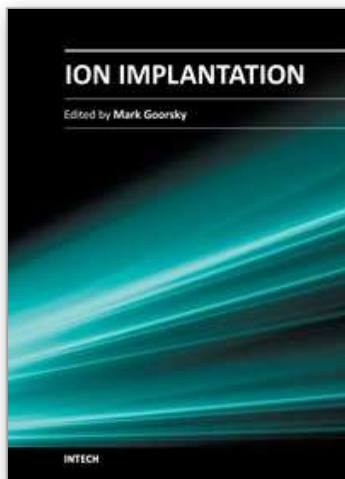
Ion Implantation

Edited by Prof. Mark Goorsky

Ion implantation presents a continuously evolving technology. While the benefits of ion implantation are well recognized for many commercial endeavors, there have been recent developments in this field. Improvements in equipment, understanding of beam-solid interactions, applications to new materials, improved characterization techniques, and more recent developments to use implantation for nanostructure formation point to new directions for ion implantation and are presented in this book.

How to reference

In order to correctly reference this scholarly work, feel free to copy and paste the following:

Stefania Maria Serena Privitera (2012). Ion Implantation in Phase Change Ge2Sb2Te5 Thin Films for Non Volatile Memory Applications, Ion Implantation, Prof. Mark Goorsky (Ed.), ISBN: 978-953-51-0634-0, InTech, Available from: http://www.intechopen.com/books/ion-implantation/ion-implantation-in-phase-change-ge2sb2te5-thin-films-for-non-volatile-memory-applications

INTECH
open science | open minds